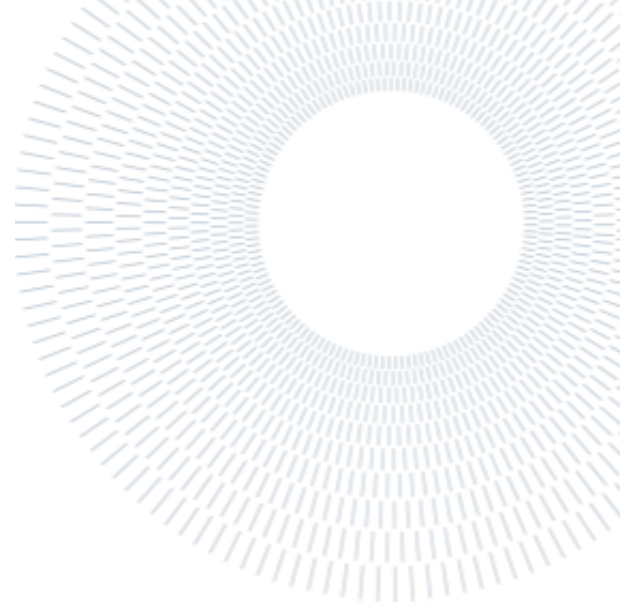




**POLITECNICO  
MILANO 1863**

SCUOLA DI INGEGNERIA INDUSTRIALE  
E DELL'INFORMAZIONE



EXECUTIVE SUMMARY OF THE THESIS

# Respiratory-Correlated (4D) Cone-Beam CT in Moving Targets Treated with Particle Therapy: a Feasibility Study for the Custom In-Room Imaging System at CNAO

TESI MAGISTRALE IN BIOMEDICAL ENGINEERING – INGEGNERIA BIOMEDICA

**AUTHOR: GLORIA SCAVOLINI**

**ADVISOR: GUIDO BARONI**

**TUTOR: GABRIELE BELOTTI**

**ACADEMIC YEAR: 2020-2021**

## 1. Introduction

Hadrontherapy is an advanced radiotherapy technique in which cyclotrons and synchrotrons accelerate charged particles with a high specific weight, forming a beam that can be directed towards the tumor. In most centers enabled for particle radiotherapy, a technique for dose delivery called *gating* is used, characterized by the periodic emission of the hadrotherapeutic beam at the end of the exhalation phase of the respiratory cycle. The choice of the emission duration, defined as *gating window*, assumes the knowledge of the uncertainty in target localization induced by the respiratory movement. The commerce of dedicated guiding devices using volumetric images for particle therapy has only recently developed<sup>1</sup> due to the complexities surrounding the installation of such systems in a hadrontherapy bunker room. The National Center for Oncological Hadrontherapy of Pavia (CNAO) has a custom in-room device for CBCT imaging, currently used for

correcting the patient's position before the start of the hadrontherapy treatment session<sup>2</sup>. This technology has additional applications, such as the respiratory correlated (4D) CBCT imaging<sup>3</sup>, which ensures the accuracy of methodologies for evaluating or adapting gated hadrontherapy treatment plans. However, an adequate acquisition protocol for optimal image quality has not been defined yet. This study aims to define binning window width, arc motion, and acquisition duration. This exploratory thesis compares the acquisitions simulated through the state-of-the-art parameters with the repeated acquisitions simulated through the parameters currently used at CNAO for 3D CBCT. Furthermore, provide a 4D CBCT acquisition procedure compatible with the CNAO environment and its clinical procedure.

## 2. Materials and methods

### 2.1. Data acquisition

In order to simulate CBCT acquisitions, the parameters of the respiratory dataset of George *et al.*<sup>4</sup> were imposed on a digital anatomical phantom (XCAT). The dataset consists of 720 samples of the antero-posterior movement of reflective markers placed on the abdomen of some patients. Then, starting from the samples of the dataset, three types of respiratory surrogates were generated. The first surrogate, called "regular", is characterized by an irregularity of 0%, having been reconstructed as a repetition of the same respiratory cycle. The second surrogate, called "verosimile" was obtained by randomly varying the width and duration of the respiratory cycle used for the first surrogate, reaching an irregularity of 1.84%. For both breath types, six surrogate signals were generated by varying the initial phase of the respiratory cycle. For the third respiratory surrogate, called "irregular", the six surrogate signals were obtained by dividing the entire dataset into six parts; they report an irregularity of 55.81%. The index is based on the calculation of the Root Mean Square Error (RMSE) of each respiratory cycle compared to the average breath of the trace in question and obtain the percentage of respiratory cycles with RMSE greater than 2 mm<sup>5</sup>.

The 2D projections (Digitally Reconstructed Radiographs - DRR) were simulated starting from the CT volumes of the XCAT phantom using the geometric parameters of CNAO CBCT system. For each respiratory surrogate sample, 5 DRRs were generated, each associated with a gantry angle, from 110° to -110°. Each acquisition contains a total of 600 DRRs.

Two acquisition sessions were subsequently performed at CNAO. A geometric phantom (ANZAI) was used in sinusoidal motion mode at 10 rpm for the first session and patient-like mode at 15 rpm. Five scans of the phantom were acquired for each session, synchronizing the start through an acoustic signal. The surrogate signal of each acquisition was obtained through the Amsterdam shroud method on the acquired projections. For the ANZAI phantom, a static scan was also acquired for each session to be used as ground truth.

### 2.2. Binning and reconstruction

For both phantoms, the 4D CBCT volumes relating to the end-inhale (EI), end-exhale (EE), 30% inhale (30%I), and 30% exhale (30%E) phases have been reconstructed, progressively adding the contribution from projection clusters of each acquisition. Each volume was reconstructed using three binning windows to assess the extent of residual anatomical movement. The binning windows used include clusters of 5, 15, and 25 projections each. The reconstructions were performed via Feldkamp-Davis-Kress implemented in RTK<sup>6</sup> and readjusted to work with CNAO data. A 3D CBCT of one acquisition was also reconstructed for both phantoms. The field of view (FOV) of CBCT reconstructions is an isocentric cylinder of dimensions 204 × 204 × 220 pixels with voxel size 1 × 1 × 1 mm.

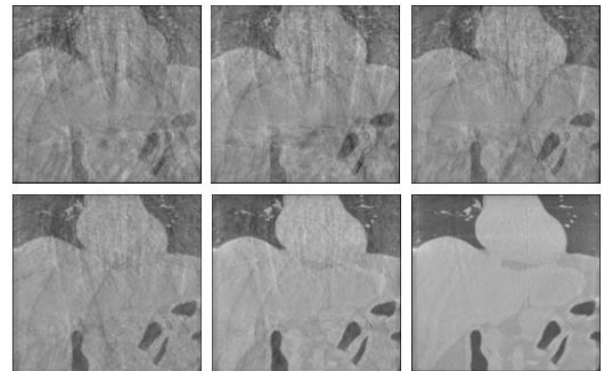


**Figure 1** Slice CBCT reconstruction XCAT phantom phase EI, regular breath, 15 projections cluster. Progressive contribution of clusters from 6 acquisitions.

### 2.3. Sampling sparsity

Image quality in 4DCBCT not only depends on the number of projections used to reconstruct, but is also influenced by the mutual location of the projection clusters used in the reconstruction. The clusters of projections must be sorted into the Bins related to the respiratory phases in which they were acquired. In the right part of Figure 2 we can see the distribution of the clusters within the first Bin, according to the source position in which they were acquired. Two different angular frequencies can be appreciated:  $1/\delta$  within the same cluster where  $\delta$  is the intra-cluster angular gap, and  $1/\Delta$  between the different clusters where  $\Delta$  is the inter-cluster angular gap. The variation of  $\delta$  does not substantially affect the final quality of the

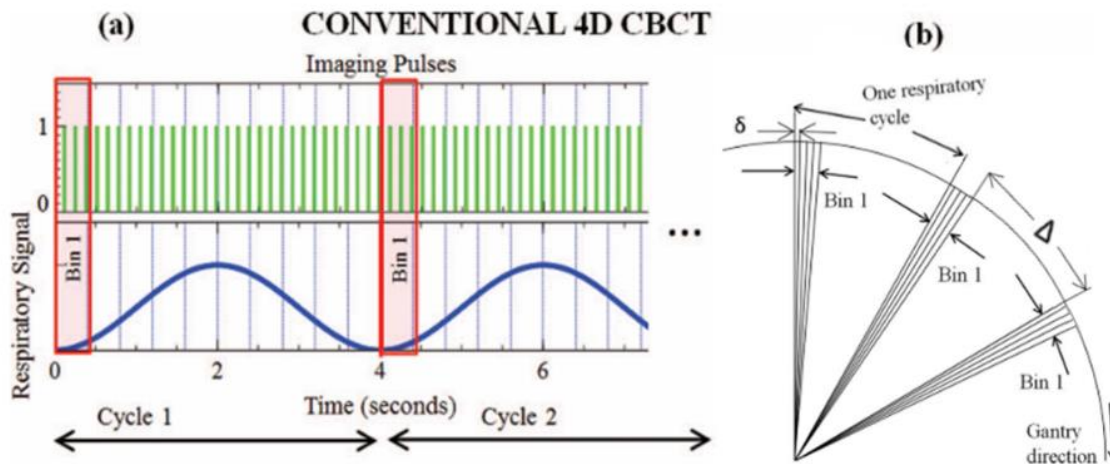


**Figure 2** Conventional 4DCBCT acquisition method: (a) sinusoidal respiratory cycle and pulse train of the projection acquisition system. Bin 1 is highlighted in red. (b) angular distribution of projection clusters belonging to Bin 1;  $\delta$  is the angular gap between adjacent projections in Bin 1;  $\Delta$  is the angular translation of the gantry in a respiratory cycle.

Source: Adapted from Cooper et al., 2013

reconstructions<sup>7-8</sup> as the projections within the same cluster carry information on the patient's anatomy similar to each other.  $\Delta$  represents the sparseness of the data and is the factor that most influences the image quality of the reconstructions as it determines the addition of the angular information of the adjacent clusters. An optimal acquisition requires that the clusters of projections are equally spaced within the rotation arc for the same respiratory Bin, ensuring the lowest possible  $\Delta$  value.

## 2.4. Slow vs. Fast acquisitions

First, the *fast* acquisition modality currently in clinical use at CNAO for 3D CBCT was compared with the state-of-art standard for 4D CBCT acquisitions, defined *slow*. At CNAO the CBCT acquisition device is calibrated to have a gantry rotation speed of  $5.4^\circ/\text{s}$ , sample frequency of 15 Hz, and a rotation arc of  $220^\circ$ . In their study, O'Brien *et al.*<sup>9</sup> report the acquisition parameters of a conventional 4D CBCT in pulse mode, with a total imaging time of 4 minutes, over a  $360^\circ$  rotation arc,  $1.5^\circ/\text{s}$  rotation speed. During a rotation, the system acquires at a frequency of 5 Hz, accumulating 1200 projections.

Given the discrepancy between the two modalities, we compared the image quality of the XCAT reconstructions obtained by simulating two repeated *fast* acquisitions and a *slow* acquisition obtained by following the guidelines of the article by O'Brien. Since CNAO CBCT Imaging System

acquires in fluoroscopic mode, it is not recommended to acquire a CBCT scan in 4 minutes as the non-therapeutic dose addressed to the patient would be unlinked from sampling frequency and only time-dependent. For this reason, we simulated an acquisition of 1200 projections. In practice, the geometry file containing the angular acquisition information was interpolated until 1200 labels were obtained, which is equivalent to halving the rotation speed of the CNAO gantry. The two techniques were compared using regular and irregular breathing patterns. The first represents the best case, in which the acquisitions can be synchronized to obtain a regular inter-cluster gap and ensure the most effective addition of information to the reconstruction. The second represents the worst case in which it is not possible to keep the inter-cluster gap constant due to irregular breathing, which could result in the addition of redundant or similar information.

## 2.5. Global metrics for image quality and Movement Artifact

The second objective is to evaluate the imaging quality of the volumes of the four respiratory phases as a function of the addition of clusters of projections from the acquisitions and the binning window used to reconstruct. The previously described *fast* mode was used for the acquisitions. Signal-to-noise ratio (SNR), contrast-to-noise ratio (CNR), mean absolute error (MAE), and cross-

correlation coefficient (CC) were evaluated on the ROIs identified in the two phantoms. The pulmonary ROI was selected for the XCAT phantom, while a spherical insert inside the cylindrical housing was selected for the ANZAI phantom. For the ANZAI phantom, a volume in the background was chosen as the background region. For the XCAT phantom, the volume relative to the liver was chosen. The MAE will be calculated only for the reconstructions related to the XCAT phantom, while for the ANZAI, HU difference will be assessed. Together with the metrics, the metrics gradients were also evaluated to highlight the addition of contribution to the metric. In this extended summary, however, just the results of MAE and HUD metrics will be reported for reasons of brevity.

The reconstructed CBCT volumes are affected by motion artifacts in proportion to the binning window used in the reconstruction. For each reconstruction containing the contribution of the clusters of all acquisitions, the residual movement of structures of interest of the phantoms will be evaluated based on the binning window used in the reconstruction.

- *Motion Blurring (MB)*: It is defined as the maximum thickness in mm of the phantom structures in the area affected by movement in the reconstructions, assessed manually through a visualization software. This metric aims to quantify the blur affecting these areas.
- *Distanza apicale (DA)*: It is defined as the maximum distance between the CBCT diaphragm profile - identified as the liver-lung separation profile - affected by motion artifact and diaphragm profile in the mean CT of the corresponding phase. It will be evaluated for the XCAT phantom only.

### 3. Results and Discussion

#### 3.1. Comparison Slow vs. Fast

In Figure 3 MAE results relating to the reconstruction of the volumes acquired in *fast* mode - in blue - and in *slow* mode - in red - are compared, depending on the reconstructed phase and the binning window. The values of all metrics

for both breath types are worse for the *slow* case than for the *fast* case for each phase and binning window. With a binning window width of 5 projections, for most metrics, the quality of *fast* reconstructions is comparable to that of *slow* reconstructions, with a slight preference for *fast* reconstructions for irregular breathing. We notice, however, that as the binning window increases, the difference between the values of the metrics of the *fast* mode compared to the *slow* one increases. This behavior can be explained by analyzing the trend of the  $\Delta$  as the binning window increases in *fast* and *slow* reconstructions. The maximum gap undergoes a reduction as the binning window width increases. This reduction, however, is more significant in *fast* acquisitions than in *slow* ones. This advantage is due to the increased speed in the rotation of the gantry, which causes the projections to have a more significant intra-cluster gap than in the *slow* case. Wider clusters mean that the *fast* protocol provides less sparse data projections in the *slow* case for the same binning window.

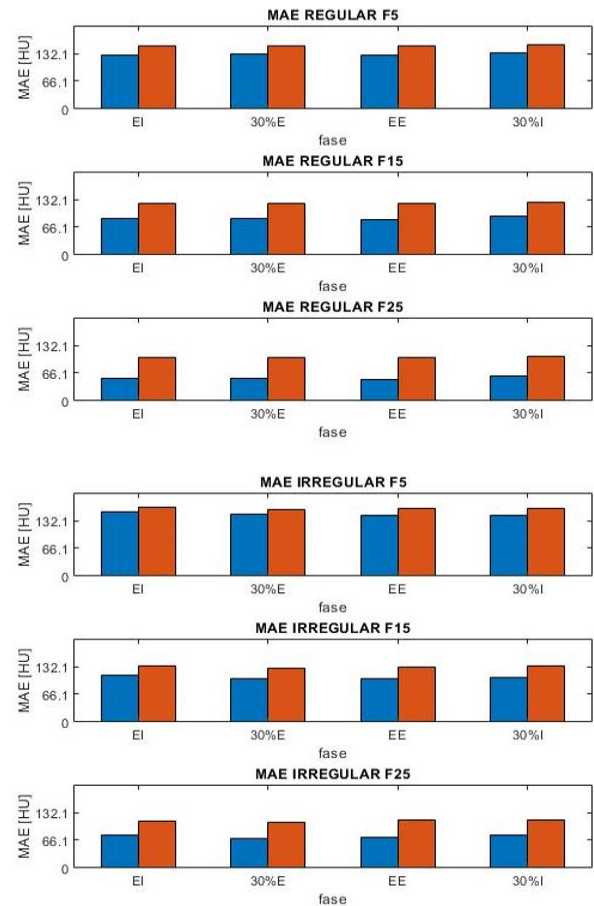


**Figure 3** MAE comparison between volumes acquired in *fast* modality - blue - and *slow* modality - red - for regular and irregular breathing.

### 3.2. Global metrics XCAT and ANZAI

In Figure 4 and Figure 5 the MAE results are reported for the XCAT and ANZAI phantom.

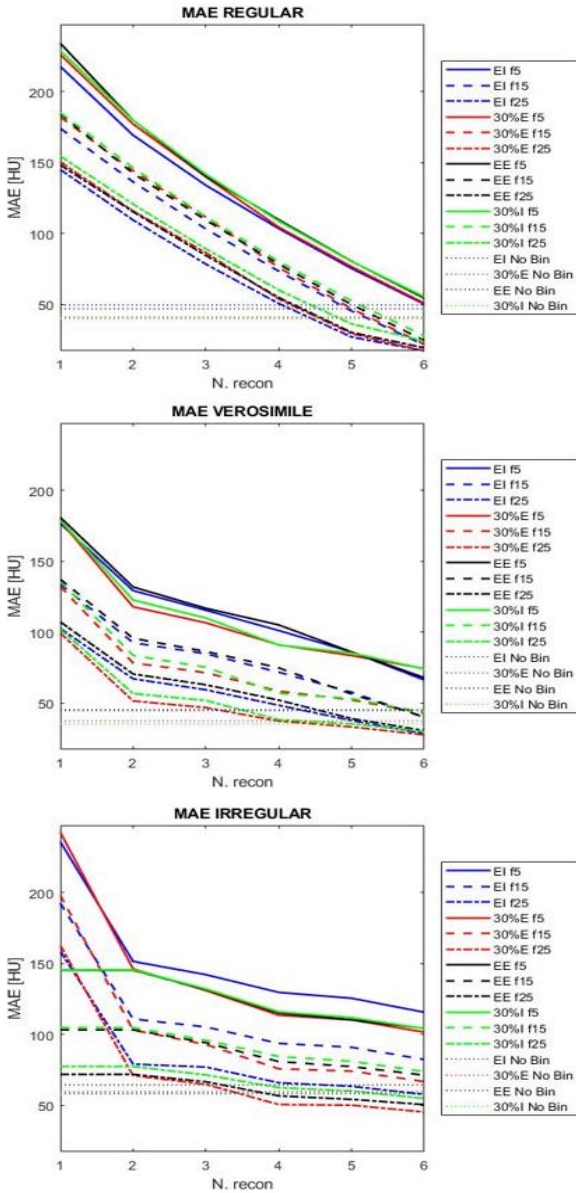


**Figure 4** MAE results for three types of breathings, XCAT phantom. Results are shown in function of the respiratory phase and binning window.

It was not possible to reconstruct the first volumes for the EE and 30%I phases for irregular breathing and the first 30%E volumes for sinusoidal motion for all binning windows due to the failure to comply with the minimum sampling condition ( $180^\circ + 2\alpha$ ; where  $\alpha$  is the fan angle). Analyzing the graphs of the metric, MAE is consistently improving as the number of acquisitions increases. We can see that there is a peak improvement

around the second reconstruction for the *verosimile* and irregular breathing. For *regular* breathing we see instead that there is a consistent addition of contribution up to the fifth reconstruction. The reconstructions with a larger binning window width report higher values of the metric compared to smaller binning window ones. The same trend is present for the *verosimile* and irregular breathing for the other metrics. The metrics' most significant addition is reached in the second progressive reconstruction, with a notable further contribution in the fourth reconstruction for the SNR case. For the *regular* case, the addition of contributions increases the metric until the fourth or fifth reconstruction.

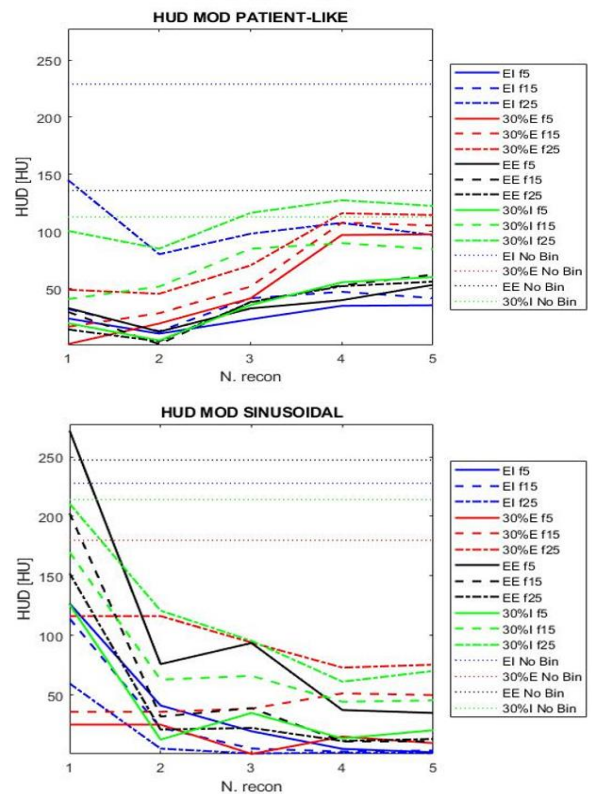


**Figure 5** HUD results for two movement modalities, ANZAI phantom. Results are shown in function of the respiratory phase and binning window.

The HUD values for each phase of the ANZAI phantom breath in sinusoidal mode decrease with increasing acquisitions. This means that the spherical inserts' mean value is getting closer to that of the static reconstruction, taken as GT. The trend is approximately constant for the patient-like mode, slightly increasing the HUD value from the second reconstruction onwards. This could be caused by some truncation artifact affecting the

spheric insert of the ground truth reconstruction. For the other metrics, the ANZAI phantom confirms the results obtained from the simulations of XCAT phantom about the quality of 4D CBCT reconstructed volumes.

### 3.3. Movement artifact results

In Table 1 are reported the MB values for each of the four breath phases evaluated manually through the visualization of volumes. For the XCAT phantom, MB values increase together with the binning window width for each breathing pattern considered. This trend is particularly evident for phases EI, 30% I and 30% E, while for EE the values remain low and approximately constant. This behavior can be explained by considering that the EE is the phase with the slightest motion of the four and the one used for the gated treatment. For this reason, it suffers from a smaller MB even for high binning windows. As for the XCAT phantom, the ANZAI phantom, for both modes, reports increasing MB values as the binning window increases.

| MB [mm] | XCAT regular |      |      | XCAT verosimile |      |      | XCAT irregular |      |      |
|---------|--------------|------|------|-----------------|------|------|----------------|------|------|
|         | F 5          | F 15 | F 25 | F 5             | F 15 | F 25 | F 5            | F 15 | F 25 |
| EI      | 0            | 1    | 1    | 0               | 2    | 3    | 0              | 4    | 6    |
| 30%E    | 0            | 2    | 4    | 0               | 3    | 5    | 0              | 2    | 2    |
| EE      | 0            | 1    | 1    | 0               | 1    | 1    | 0              | 1    | 2    |
| 30%I    | 1            | 2    | 6    | 0               | 3    | 7    | 0              | 2    | 4    |
| No Bin  | 7            |      |      | 7               |      |      | 10*            |      |      |

| MB [mm] | ANZAI sinusoidal |      |      | ANZAI patient-like |      |      |
|---------|------------------|------|------|--------------------|------|------|
|         | F 5              | F 15 | F 25 | F 5                | F 15 | F 25 |
| EI      | 0                | 0    | 1    | 0                  | 2    | 4    |
| 30%E    | 3                | 8    | 9    | 1                  | 2    | 5    |
| EE      | 0                | 0    | 1    | 0                  | 1    | 2    |
| 30%I    | 2                | 7    | 10   | 2                  | 6    | 9    |
| No Bin  | 19               |      |      | 19                 |      |      |

**Table 1** MB for XCAT and ANZAI phantoms. The results are shown as a function of the respiratory phase and the binning window for the last reconstruction. \*Mean value.

As seen in Table 2, DA also tends to increase with the binning window width for all breathing patterns considered. We can see how the DA has a much lower range of values for the EE than for the other phases, while, on the other hand, it reports very high values for the EI phase. This depends on the fact that the CBCT diaphragm profile manually segmented to calculate the DA is more representative of EE than that of the other phases, since EE is the most consistent phase. This demonstrates, once again, the effectiveness in operating gating during the EE phase, as the 4D CBCT reconstructions of this phase are minimally affected by the movement artifact, even in the case of large binning windows. For the remaining three phases, the evaluation of the MB is more significant.

| DA [mm] | XCAT regular |      |      |        | XCAT verosimile |      |      |        | XCAT irregular |      |      |        |
|---------|--------------|------|------|--------|-----------------|------|------|--------|----------------|------|------|--------|
|         | F 5          | F 15 | F 25 | No Bin | F 5             | F 15 | F 25 | No Bin | F 5            | F 15 | F 25 | No Bin |
| EI      | 0            | 1    | 3    | 7      | 0               | 1    | 3    | 8      | 1              | 3    | 5    | 13*    |
| 30%E    | 1            | 2    | 2    | 2      | 1               | 2    | 3    | 2      | 1              | 2    | 3    | 2*     |
| EE      | 1            | 0    | 1    | 1      | 1               | 1    | 1    | 0      | 1              | 1    | 2    | 1*     |
| 30%I    | 0            | 3    | 2    | 3      | 1               | 1    | 4    | 4      | 0              | 2    | 3    | 2*     |

**Table 2** DA phantom XCAT of the three types of breath. The results are reported as a function of the respiratory phase and the binning window for the sixth reconstruction. \*Mean value.

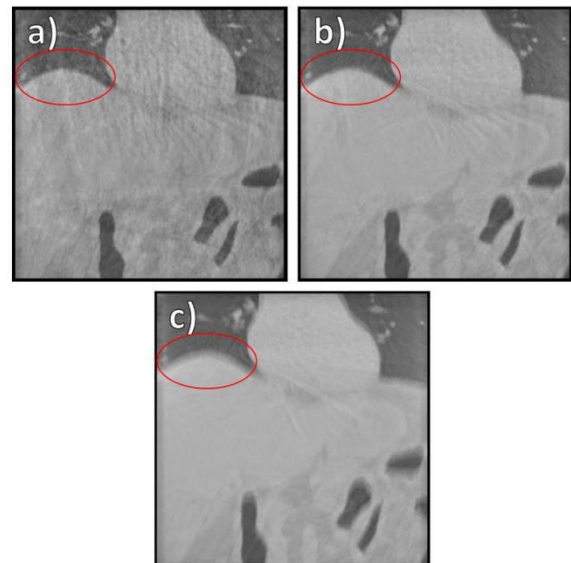


**Figure 5** Sixth progressive reconstruction of the XCAT phantom, regular breathing. a) 5-Binning window; b) 15-Binning window; c) 25-Binning window. Increasing Motion blurring is circled in red.

## 4. Conclusions

The results comparing the *fast* and *slow* acquisition methods highlight how *slow* acquisitions provide lower imaging quality than *fast* acquisitions. However, the latter must be acquired with good synchronization to minimize the inter-cluster gap and make it uniform. In the literature, studies regarding *fast* repeated 4D CBCT acquisitions are not known. For this reason, we believe that the results found here can provide a starting point for the definition of a new clinical standard for 4D CBCT acquisitions, especially with fluoro systems. The global metrics for the evaluation of imaging quality obtained for the XCAT phantom show how most of the improvement to the final image occurs from the third to the fourth acquisition. As for the binning window width, 5 projections per cluster results in residual motion at resolution limit in the more stable phases. However, they are not sufficient to achieve satisfactory image quality. Binning window width at 25 projections guarantees the best metric values. However, the use of such a wide binning window involves the presence of high residual movement, especially regarding the 30% E and 30% I phases. To limit the acquisition time with the aim of reducing the non-therapeutic X-ray dose directed to the patient, the acquisition of three rotations of the CBCT gantry is considered sufficient to obtain good imaging quality. As for the recommended binning window, the choice must be related to the purpose of 4D CBCT imaging. In contexts involving the qualitative evaluation of reconstructed volumes or DIR applications, a binning window of 15 projections is advisable. Undoubtedly, a software viewer could allow the clinician to quickly scroll between different reconstructed phases and between different windows for a specific phase. In conclusion, CNAO can now have a tool capable of acquiring CBCT projections in a tailored protocol, which provides added value to the standard found in the literature. CNAO technicians will have immediate access to a 4D CBCT acquisition method for qualitative assessments of the patient's anatomy and have the opportunity to direct further studies in the implementation of the tool for adaptive radiotherapy approaches.

## 5. Bibliography

1. Landry G, Hua C ho. Current state and future applications of radiological image guidance for particle therapy. *Med Phys.* 2018;45(11):e1086-e1095. doi:10.1002/mp.12744
2. Hua C. Full Paper A robotic C-arm cone beam CT system for image- guided proton therapy: design and performance. 2017;(April).
3. Hugo GD, Rosu M. Advances in 4D radiation therapy for managing respiration: Part I - 4D imaging. *Z Med Phys.* 2012;22(4):258-271. doi:10.1016/j.zemedi.2012.06.009
4. George R, Chung TD, Vedam SS, et al. Audio-visual biofeedback for respiratory-gated radiotherapy: Impact of audio instruction and audio-visual biofeedback on respiratory-gated radiotherapy. *Int J Radiat Oncol Biol Phys.* 2006;65(3):924-933. doi:10.1016/j.ijrobp.2006.02.035
5. Paganelli C, Portoso S, Garau N, et al. Time-resolved volumetric MRI in MRI-guided radiotherapy: An in silico comparative analysis. *Phys Med Biol.* 2019;64(18). doi:10.1088/1361-6560/ab33e5
6. Rit S, Vila Oliva M, Brousmiche S, Labarbe R, Sarrut D, Sharp GC. The Reconstruction Toolkit (RTK), an open-source cone-beam CT reconstruction toolkit based on the Insight Toolkit (ITK). *J Phys Conf Ser.* 2014;489(1):1-4. doi:10.1088/1742-6596/489/1/012079
7. Cooper BJ, O'Brien RT, Balik S, Hugo GD, Keall PJ. Respiratory triggered 4D cone-beam computed tomography: A novel method to reduce imaging dose. *Med Phys.* 2013;40(4):1-9. doi:10.1118/1.4793724
8. Maurer J, Pan T, Yin FF. Slow gantry rotation acquisition technique for on-board four-dimensional digital tomosynthesis. *Med Phys.* 2010;37(2):921-933. doi:10.1118/1.3285291
9. O'Brien RT, Cooper BJ, Keall PJ. Optimizing 4D cone beam computed tomography acquisition by varying the gantry velocity and projection time interval. *Phys Med Biol.* 2013;58(6):1705-1723. doi:10.1088/0031-9155/58/6/1705